Tidal Energetics over the Chatham Rise, New Zealand

STEPHEN M. CHISWELL

National Institute of Water and Atmospheric Research, Wellington, New Zealand

12 July 1999 and 2 March 2000

ABSTRACT

Separate one-month current meter deployments in 1996 and 1997 over the Chatham Rise, east of New Zealand, show that tidal phases are both stable in time and close to those derived from a barotropic tidal model, while amplitudes show coefficients of variation as high as 30%. These observations are consistent with the presence of a baroclinic component to the tide that is phase-locked to the barotropic component. The near-zero phase difference between the model and observations suggests local generation of the barotropic tide. As well as the current meter data, two 24-hour time series of CTD casts are used to compute tidal vertical displacements. Vertical displacements up to 40 m lead to estimates of time-averaged potential energy ranging from 75 to 782 J m^{-2} for the semidiurnal tide and 40 to 147 J m^{-2} for the diurnal tide. Energy radiated from the Chatham Rise could be as high as 1.1 GW.

1. Introduction

Baroclinic tides are increasingly being regarded as a source of global ocean energy dissipation. Munk and Wunsch (1998) calculate that a mean diffusivity of 10^{-4} m^{-2} s^{-1} is required throughout the world's oceans in order for the upward advection of deep water to be balanced by downward diffusion of heat, but comment that most open ocean measurements of diffusion are an order of magnitude less than this. Munk (1998, personal communication) argues that the dissipation of the baroclinic tide results in the production of shear-unstable internal waves and suggests that much of the missing dissipation could be near regions of steep topography where baroclinic tide energy is expected to be large. Munk and Wunsch (1998) calculate that about 800 to 1800 GW of energy dissipation are required beyond that provided by pelagic diffusion.

Much of the early work on baroclinic tides suggested that they are highly incoherent in both space and time. For example, Radok et al. (1967) found baroclinic tides in the eastern Pacific to have random phase, and ascribed this to variations in the thermal structure. Similarly, Magaard and McKee (1973) found the phase of first- and second-mode baroclinic M_2 tides to vary by 100° over time, compared to 10° for the barotropic component. Barnett and Bernstein (1975) found horizontal coherence of tidal temperature perturbations only on scales less than 50 km.

However, there is a body of opinion (e.g., Hendry 1977) that suggests the baroclinic tide should be generated with constant phase relative to the barotropic tide, that is, that the baroclinic tide is phase-locked to the barotropic tide. This phase may later be distorted by buoyancy frequency variations or currents. There is evidence to suggest that a significant coherent component to the baroclinic tide exists, for example, Dushaw et al. (1995) used a tomographic array (~1000-km side), to observe a coherent M_2 baroclinic tide about 2000 km from the Hawaiian Islands. Chiswell and Moore (1999) have shown that the Kermadec Ridge northeast of New Zealand is a source of coherent baroclinic tidal energy, calculating that it radiates about 0.8 GW power. Further evidence that a significant component of the baroclinic tides is generated phase-locked with the barotropic tides comes from TOPEX/Poseidon altimetric measurements. Ray and Mitchum (1996) report a coherent tide propagating to the northeast from the Hawaiian Ridge.

Kantha and Tierney (1997) comment that midocean ridges that are shallow and whose crests are perpendicular to the barotropic currents are expected to be quite efficient in generating baroclinic currents. The Chatham Rise, which extends out to the east of New Zealand, has a sill depth of about 350 to 400 m, and previous work (Heath 1977) shows that the M_2 cophase lines run approximately parallel to the crest of the rise. Thus, it may be that the Chatham Rise is also a source of baroclinic tides. If this is so, it is desirable to compute the baroclinic tide levels there.

As part of an interdisciplinary study of the subtropical

Corresponding author address: Dr. Stephen M. Chiswell, National Inst. of Water and Atmos. Res. Ltd., 301 Evans Bay Parade, Greta Point, P.O. Box 14-901, Kilbirnie, Wellington, New Zealand.
E-mail: s.chiswell@niwa.cr.nz

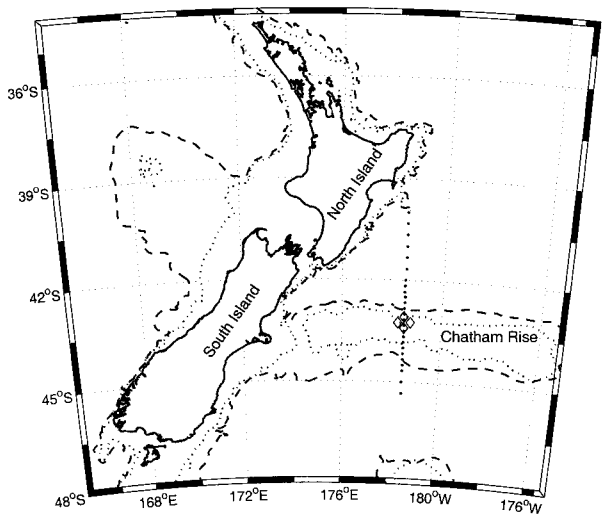

FIG. 1. Map showing location of 1996 and 1997 current meter array (diamonds). Dots show CTD transect made in May 1997. The 24-h time series in May 1997 and Apr 1999 were made within the array. The 1000-m and 500-m isobaths are shown as dashed and dotted lines.

front over the Chatham Rise, two separate one-month-long deployments of an array of current meters were made near its crest 1996 and 1997 (Fig. 1). As well as these current meter data, on two separate occasions, time series of CTD casts spanning 24 hours were made within the array. The first time series was made during 31 May 1997, the second during 16 April 1999.

In this paper, I use these data to make preliminary estimates of the baroclinic tide and investigate two questions.

1) What are the energy levels of the baroclinic tide—can the Chatham Rise generate significant baroclinic tide to contribute to the global tidal budget? and
2) Is the baroclinic tide, assuming it exists, phase-locked to the barotropic tide? If so, this would suggest a structured large-scale mechanism for baroclinic tide generation (e.g., Baines 1982).

Separating baroclinic from barotropic tides in current meter data, especially with poor vertical resolution is notoriously difficult. Other researchers (e.g., Levine and Richman 1989; Chiswell and Moore 1999) have used longer time series and/or better vertical resolution to tackle this problem. Here I take a different approach. Dealing with question 2 first, I show that computed phases from the current meters in 1996 and 1997 are essentially the same, and compare well with barotropic model results of Walters and Goring (2000, manuscript submitted to *J. Geophys. Res.*, hereafter WG). Coefficients of variation in the amplitudes range from 19% to 30%. Traditionally, such high variability in tidal constituents is attributed to the presence of incoherent energy in the records, but a Monte Carlo simulation shows that this explanation cannot be used to account for the variability seen here. Instead, I interpret these results to invoke a conceptual model that a baroclinic tide exists and is phase-locked to the barotropic tide with near-zero phase, but that its amplitude varies.

Then I use the CTD time series data to fit diurnal and semidiurnal harmonics to the temperature profiles and use these to compute the vertical displacements of the baroclinic tide. The potential energy associated with the baroclinic tide is computed from these displacements functions. Kinetic energies for both baroclinic and barotropic tides are computed using the conceptual model of the tides, plus the assumption that the numerical model of WG can be used to determine the barotropic tide.

2. Methods

a. Tidal model results

The numerical model results are derived from a finite-element barotropic model. Output from the model is amplitude and phase of the five major tides at each grid point. Tidal parameters from the grid point closest to the array (about 6 km from the array center) are used here.

b. Current meter data

During May 1996, a diamond-shaped array of current meter moorings was deployed over the crest of the Chatham Rise near 178°30′E (Fig. 1). This array was recovered after a month. A second month-long deployment in nearly the same location was made in October 1997. During both deployments, current meters were placed at nominal depths of 120 and 250 m.

Tidal constituents were computed for each record using a harmonic analysis package (TASK) provided by the U.K. Permanent Service for Mean Sea Level at the Proudman Oceanographic Laboratory. With approximately one month of data 27 tidal constituents are computed, and the major diurnal and semidiurnal components can be separated. Five major tides (M_2, S_2, N_2, O_1, and K_1) are considered here. Tidal constituents are discussed in terms of the ellipse parameters: Amplitude, A, is the semimajor axis length; eccentricity, e, is $\sqrt{(A^2 - B^2)/A^2}$ (B is the semiminor axis length); orientation of ellipse, ϕ, is with respect to north; and Greenwich phase, g, is phase of maximum current having a northgoing component.

c. Hydrography

The large-scale hydrography was mapped with a section extending from 40° to 45°20′S (Fig. 1) in both May 1997 and April 1999. As well as this section, during both cruises, CTD casts were made at a fixed site within the array at approximately 3-h intervals over 24 hours. During May 1997 nine casts were made at 43°15′S, 178°20′E. During April 1999, 14 casts were made at 43°18′S, 178°30′E.

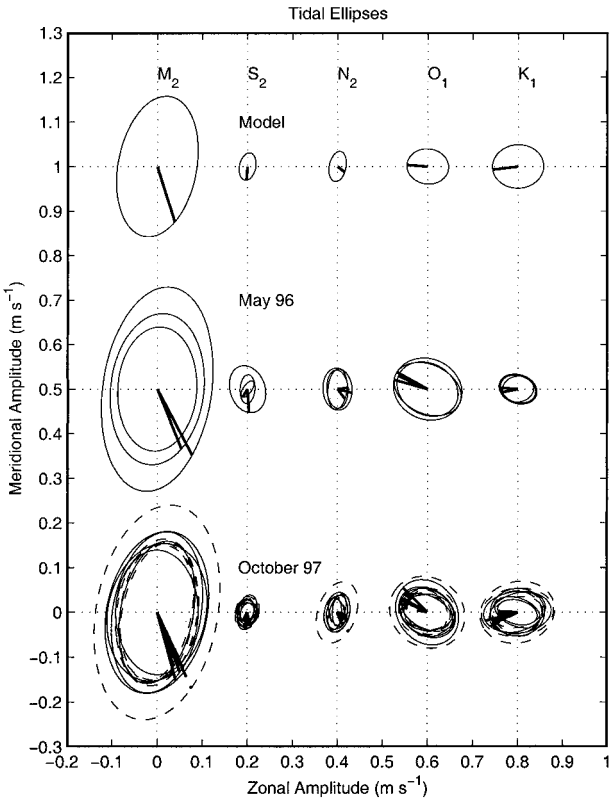

FIG. 2. Tidal ellipses for five major tides. The top row shows ellipses from the Walters and Goring model. Remaining rows show ellipses from 1996 and 1997 deployments. Solid lines show ellipses from 120 m; dashed lines show ellipses from 250 m.

A Seabird CTD (conductivity–temperature–depth) profiler in a 12-place rosette with 1.2 L Niskin bottles was used to make continuous vertical profiles of temperature and salinity at each station. Water samples were collected to calibrate the conductivity sensor. CTD data collection and processing methods were the same as those detailed in Chiswell et al. (1993) and Walkington and Chiswell (1998). Temperature, *T,* and salinity, S, were processed to 2-dbar bins. Temperature is estimated to be accurate to 3m°C, salinity to 5 m psu.

3. Results

a. Horizontal currents

All ten current meters from the 1997 deployment, and four of eight meters from the 1996 deployment returned complete datasets. Tidal constituents for each of these 14 records were completed independently as described in the methods section. The resulting tidal ellipses for the five major tides from all 14 records are plotted in Fig. 2, along with those derived from the model. Mean amplitude, eccentricity, orientation and phase for each of the five major tides are summarized in Table 1, along with these parameters from the Walters and Goring model for the array location.

TABLE 1. Amplitudes A, eccentricities ε, orientations ϕ, and phases g, for the five major tides over the Chatham Rise.

Tidal constituent		Model	Observed		
			Mean	Std dev.	Coefficient of variation
M_2	A (cm s^{-1})	16	17.1	3.1	0.18
	ε	0.839	0.815	0.045	0.055
	ϕ (°)	10	7.8	3.3	
	g (°)	137	133	8.0	
S_2	A	3.11	3.11	0.82	0.26
	ε	0.813	0.74	0.13	0.17
	ϕ	11	7.7	17	
	g	169	174	17.3	
N_2	A	3.42	4.09	1.2	0.29
	ε	0.838	0.838	0.062	0.074
	ϕ	10	3.4	13	
	g	106	112	12.7	
O_1	A	4.65	6.68	1.2	0.17
	ε	0.534	0.625	0.1	0.17
	ϕ	−82	−60	42	
	g	−4	0	46.5	
K_1	A	5.69	5.6	1.6	0.28
	ε	0.514	0.683	0.11	0.16
	ϕ	88	51	76	
	g	175	−175	82.2	

The dominant tide, as expected (Chiswell 1994; Goring et al. 2000, manuscript submitted to *N. Z. J. Mar. Freshwater Res.*; Heath 1977), is the M_2 tide, having amplitudes of around 17 cm s^{-1}. Eccentricities are about 0.84, and ellipse orientations are slightly east of north. The next strongest semidiurnal tide is the N_2 tide, having amplitudes of about 4 cm s^{-1}, followed by the S_2 tide with amplitudes about 3 cm s^{-1}. As Heath (1977) has previously shown for the Chatham Rise, the diurnal tides are strong, with the O_1 and K_1 tides having amplitudes about 6 cm s^{-1} (i.e., twice that of the S_2 tide). The diurnal tides are less eccentric than the semidiurnal tides, with eccentricities about 0.5, and orientations are aligned more along the ridge than for the semidiurnal tides. For most tides, mean observed amplitudes are slightly greater than predicted by the model (e.g., 17.1 vs 16.0 cm s^{-1} for the M_2 component). Phase differences between the model and mean observed are $<5°$. Eccentricities and orientations also agree well.

With 14 separate observations there is considerable scatter in some computed tidal constituents; for example, the coefficient of variation (standard deviation/mean) of amplitude ranges between 17% and 29%, depending on the tide (Fig. 3). The standard deviation in phase ranges from 8° to 18°. As Fig. 2 suggests, but not shown explicitly here, there is as much variation within each year (i.e., across the array) as between years, and there are no significant differences in the tidal constituents either with depth or between our 1996 and 1997 deployments.

Scatter in tidal constituents is commonly seen in current meter observations and is usually attributed (e.g., Pugh 1987) to the presence of incoherent ''noise'' in

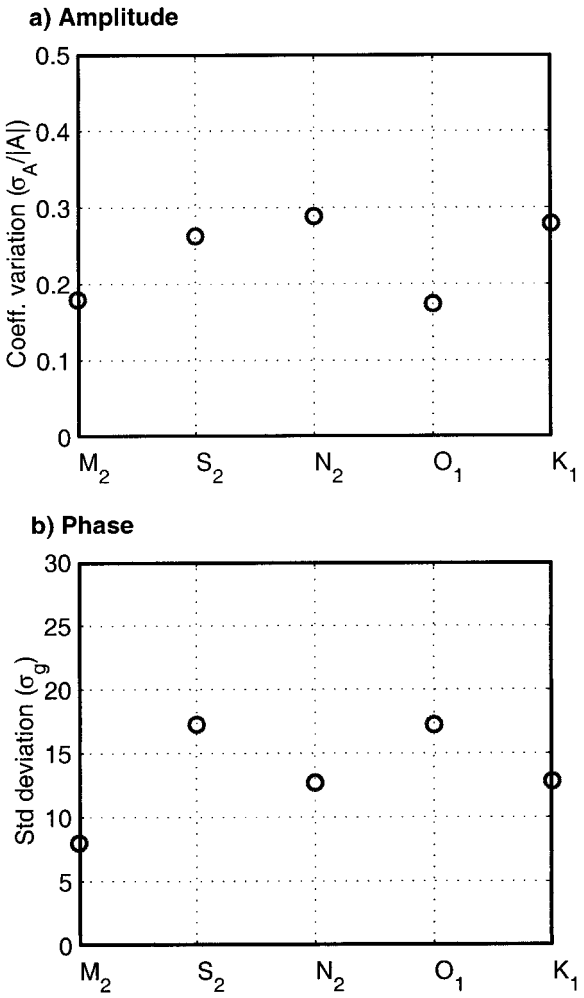

FIG. 3. (a) Coefficient of variation of the 14 estimates of semimajor amplitudes for each of the five principal tides; (b) as in (a) but for standard deviation of phase.

the tidal band—the more uncorrelated noise, the higher the standard error in the tidal constituents. Thus, the observed scatter in the tidal constituents seen here could simply be the result of a high degree of incoherent tidal energy. However, one can directly test this explanation by using a Monte Carlo simulation to calculate the incoherent energy level required to produce the observed scatter in tidal constituents, and then comparing this level with observed incoherent energy levels determined from observed coherence-squared between records.

One hundred simulations of one-month long analyses were made at each of several noise levels, allowing one to plot the coefficient of variation (or standard deviation where appropriate) of each tidal parameter against incoherent energy level. To reproduce the observed coefficient of variation of 19% in the M_2 amplitude requires a ''noise-to-signal ratio'' of 55, whereas to reproduce the 8° standard deviation seen in the M_2 phase requires a noise-to-signal ratio of 10. (Note: The noise-to-signal ratio is defined here as the variance of the noise divided by the variance of the tide. Since the tide is a sinusoid, whereas the noise is broadband, the noise-to-signal ratio over the tidal band is subject to definition of the width of the tidal band, but will be less.) Observed coherence-squared falls within the 95% confidence limits predicted for a noise-to-signal ratio of 10, but outside those for a noise-to-signal ratio of 55.

Thus the observed scatter in phase is within that expected given the observed coherence between records, but the scatter in tidal amplitude is much higher. Consequently, one cannot explain the observed variability in tidal amplitudes as due to the presence of uncorrelated energy in the tidal band. Instead, these results support a conceptual model that the baroclinic tides are phase-locked to the barotropic tide, but are generated with varying amplitude. That the observed phase is close to that predicted by the Walter and Goring model suggests (but does not confirm) that the tide is generated locally.

Such a hypothesis is not unique here, for example, Mitchum and Chiswell (2000, manuscript submitted to *J. Geophys. Res.*; hereafter MC) find that (at much longer timescales) internal tide amplitudes vary as the local thermal structure changes due to the passage of Rossby waves. It may be that the variability in the tidal constituents seen over the Chatham Rise reflects changes in the baroclinic generation associated with array-scale variability within the subtropical front. In the remainder of this article, the baroclinic tides are assumed to follow this conceptual model.

b. Vertical tidal displacements

Figures 4 and 5 summarize the hydrological data from the two cruises in May 1997 and April 1999. In each case, temperature from the large-scale section along 178°30′E is shown; also shown are temperature versus salinity (*T–S*) for the large-scale section with *T–S* from the 24-h time series superimposed, and time–depth contours of temperature and salinity from the 24-h time series.

Temperature–salinity from the large-scale sections shows an envelope of *T–S* ranging from relatively warm and saline subtropical waters to relatively cool and fresh subantarctic waters. Below the sill depth, the Chatham Rise acts as a barrier to mixing, and the *T–S* separates into two distinct curves in the Antarctic Intermediate Water. Despite both cruises occurring at about the same time of the year, there are considerable differences in the structure of the subtropical front. Compared to 1997, in 1999 surface temperatures were up to 3°C warmer, thermal gradients within the subtropical front were stronger, and the front showed a double front (illustrated by the voids in the *T–S* envelopes).

During both 1997 and 1999, the 24-h time series were made south of the main front. In both cases, *T–S* from the 24-h CTD time series shows little variability below

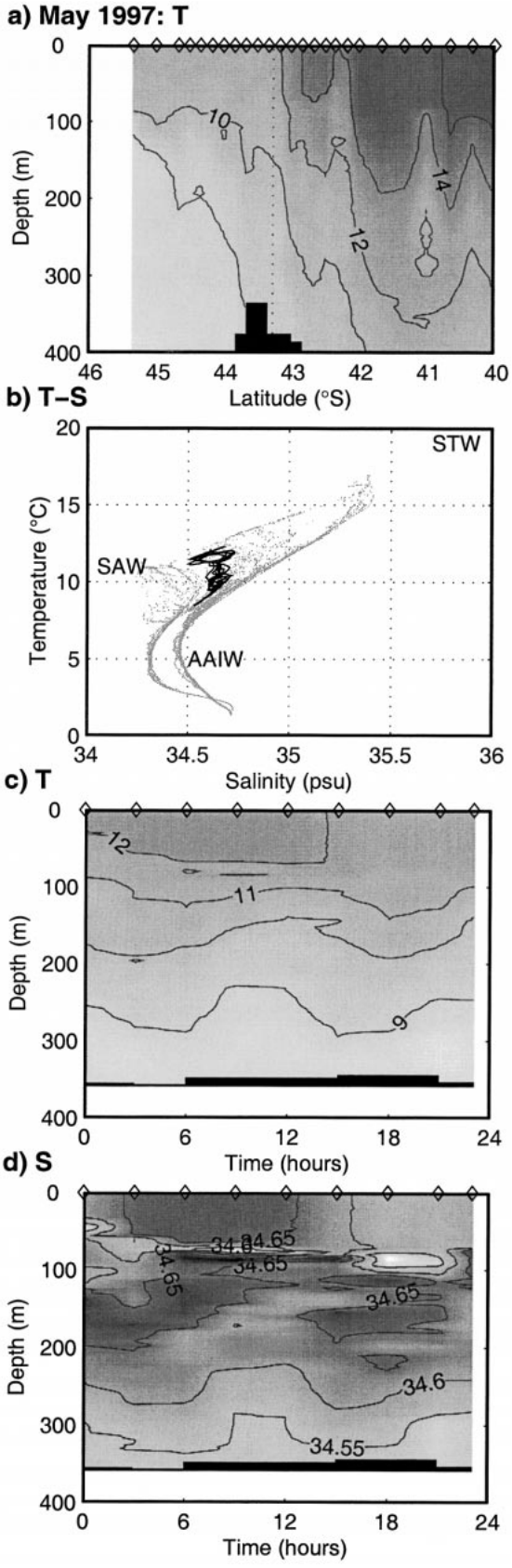

about 200 m, but above this level salinity at any given temperature varies by up to 0.2 psu.

Temperature and salinity from the 24-h CTD time series (panels c and d in Figs. 4 and 5) show that during both years, the mixed layer extended to about 50–70 m; however below this depth, individual isotherms and isohalines show oscillations that are correlated in temperature and salinity. For example during May 1997, the 9°C isotherm and the 34.6 psu isohaline appear nearly identical. Isotherm and isohaline oscillations during May 1997 appear to show a strong semidiurnal component; for example, the 10°C shows about a 50-m peak-to-peak excursion (from 120 to 170 m). Compared to the earlier cruise, the April 1999 shows less obvious evidence of semidiurnal tidal oscillations.

Meridional temperature gradients derived from the large-scale section at the depths of the current meters are about 1.4×10^{-5} °C m^{-1}. A scale analysis, not shown here, confirms that these gradients are too low for horizontal advection to be the cause of these oscillations, and one can assume that they are due solely to vertical motion induced by the baroclinic tide.

During the 24-h CTD time series, it is assumed that temperature T is governed solely by vertical perturbation of the mean field so that

$$T(z, t) = \overline{T}(z) - \eta(z, t)\frac{\partial \overline{T}(z)}{\partial z}, \qquad (1)$$

where η is the internal vertical displacement. Here the z direction is taken as positive upwards.

Temperature and the vertical displacement can also be written in terms of a mean, diurnal and semidiurnal tides, and residual:

$$\begin{aligned} T(z, t) &= \overline{T}(z) + T_1(z)\cos(\omega_1 t - \phi_1^T(z)) \\ &\quad + T_2(z)\cos(\omega_2 t - \phi_2^T(z)) + \varepsilon^T \\ \eta(z, t) &= \eta_1(z)\cos(\omega_1 t - \phi_1^\eta(z)) \\ &\quad + \eta_2(z)\cos(\omega_2 t - \phi_2^\eta(z)) + \varepsilon^\eta, \end{aligned} \qquad (2)$$

where ω_1 and ω_2 are taken here as the frequencies of the diurnal (~24 h) and semidiurnal (12.4206 h) tides. Note that the mean vertical displacement is zero.

By collecting terms at each frequency, the vertical displacements for each tidal constituent can be estimated by dividing the amplitude functions by the mean vertical gradient. In order to keep the amplitudes (T and η)

←

FIG. 4. Hydrographic data collected in May 1997: (a) Temperature section from 40° to 45°20′S. Black region indicates the Chatham Rise. Diamonds along upper axis show CTD cast locations. The vertical dotted line near 43°S indicates the location of the current meter array and the 24-h time series site. (b) Temperature–salinity plot for 24-h CTD time series (black) superimposed on T–S for section shown in (a). (c) Temperature from the 24-h CTD time series. Diamonds along upper axis show CTD cast times. (d) Salinity from the 24-h CTD time series.

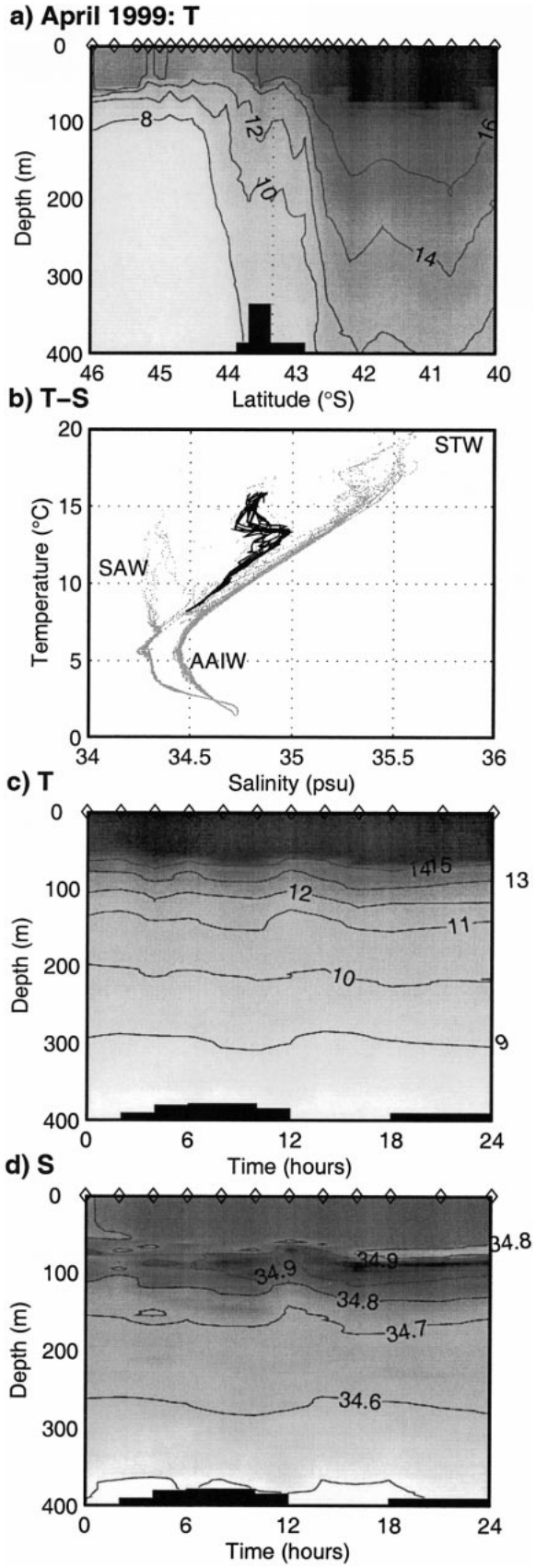

positive, the negative sign in (1) is incorporated as a phase change:

$$\eta_1(z) = \frac{T_1}{\partial\overline{T}/\partial z}, \qquad \eta_2(z) = \frac{T_2}{\partial\overline{T}/\partial z},$$
$$\phi_1^{\eta} = \phi_1^{T} + \pi, \qquad \phi_2^{\eta} = \phi_2^{T} + \pi. \tag{3}$$

Similar equations hold for salinity, and density, but, because salinity passes through a maximum near 100 m and is inherently noisier than temperature, the salinity-derived functions are much noisier than those derived from temperature.

Vertical displacement functions and phase for the tides derived from temperature are shown in Fig. 6. During 1997, semidiurnal vertical displacement amplitudes below the mixed layer ranged from about 20 to 50 m. Peak amplitudes occurred at about 150-m depth. Diurnal amplitudes are about ⅓ those of the semidiurnal tide, which is approximately the ratio of the diurnal to semidiurnal tidal currents. The diurnal displacement functions appear to be bottom trapped. Below 100 m, both semidiurnal and diurnal phase increases from the bottom toward the surface, the sense of this phase change is such that vertical displacement occurs later higher in the water column—note that the phase origin here is arbitrary.

During 1999, both diurnal and semidiurnal amplitudes were considerably less than those seen in 1997. Semidiurnal amplitudes below the mixed layer were about 10 m. Again, diurnal amplitudes were less than semidiurnal amplitudes. As in 1997, the displacement functions show a slight tendency towards bottom trapping. The semidiurnal phase propagates vertically in the opposite direction compared to 1997, and the diurnal phase shows little vertical change.

c. Energetics

Each 24-h CTD data time series can be used to estimate the potential energy due to the baroclinic tide over two tidal cycles, but the baroclinic kinetic energy cannot be calculated directly because of the difficulty in separating the baroclinic and barotropic currents. However, if the Walters and Goring model is assumed to be accurate, one can use it directly to estimate the barotropic energies. Baroclinic kinetic energies are calculated assuming the conceptual model described above.

1) BAROTROPIC ENERGIES

Potential and kinetic energies for the barotropic tide can be estimated from the model:

←

FIG. 5. As in Fig. 4 but for Apr 1999.

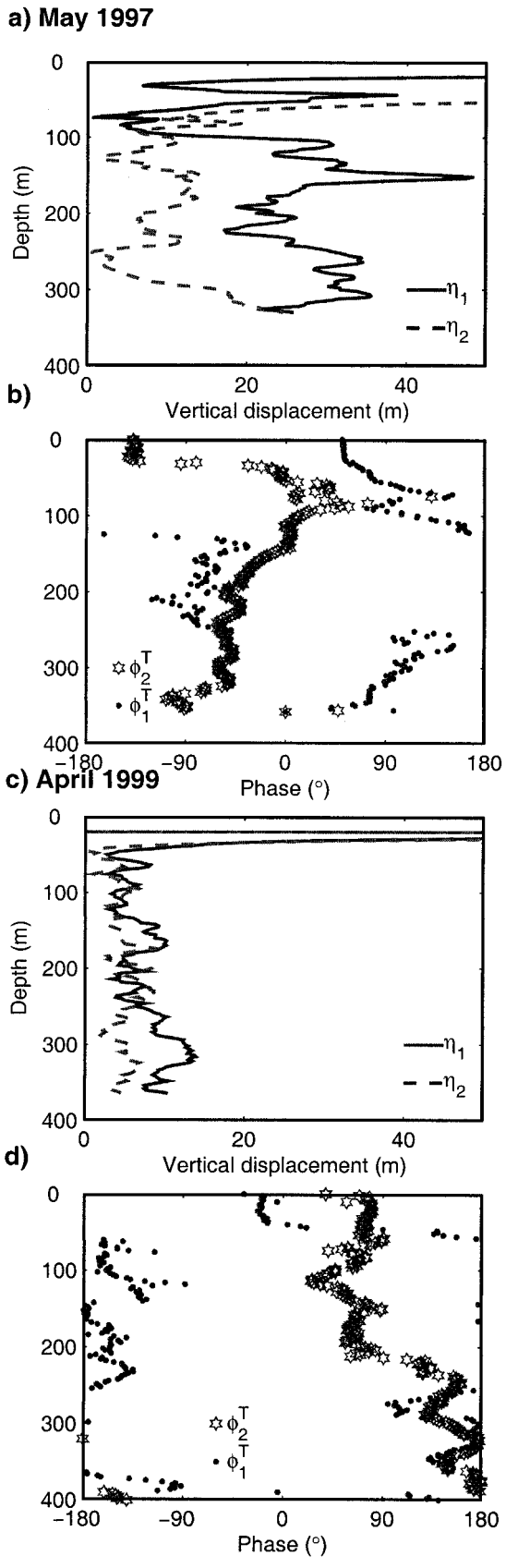

$$\langle \mathrm{PE} \rangle = \frac{1}{2T} \int_0^T \rho g \eta^2(t)\, dt \quad \text{and}$$

$$\langle \mathrm{KE} \rangle = \frac{1}{2T} \int_0^T \rho H(u^2(t) + v^2(t))\, dt, \qquad (4)$$

where η, u, and v are surface elevation, and barotropic currents, respectively; ρ is density, and H is the water depth. Because of beating between the tides, semidiurnal and diurnal energies are modulated. Long-term mean kinetic and potential energies are respectively 1578 and 747 J m^{-2} for the semidiurnal tides and 420 and 3.9 J m^{-2} for the diurnal tides (Table 2).

2) Baroclinic potential energy

Once the displacement profile is determined, the potential energy density due to the baroclinic tide can be determined by (e.g., Dushaw et al. 1995)

$$\langle \mathrm{PE} \rangle = \frac{1}{T} \int_0^T \frac{1}{2} \int_{-H}^0 \rho(z) N^2(z) \eta^2(z, t)\, dz\, dt, \qquad (5)$$

where η is the displacement profile, N is the Brunt–Väisälä frequency, and ρ is density.

Table 3 shows the results obtained from these cruises neglecting the upper mixed layer where η is poorly defined. For the 1997 cruise, the mean potential energy determined here is 782 J m^{-2} for the semidiurnal tide and 147 J m^{-2} for the diurnal tide. For the 1999 cruise, these numbers are reduced considerably to 75 J m^{-2} and 40 J m^{-2}, respectively. The barotropic energies for the respective 24-h time periods in 1997 and 1999 had about a factor of 2 difference. This suggests that not all the difference between the 1997 and 1999 results can be accounted for by modulation of the driving barotropic tides, possibly indicating different barotropic-to-baroclinic conversion rates during the two time periods.

3) Baroclinic kinetic energy

The baroclinic currents were estimated by reconstructing semidiurnal and diurnal currents from the observed tidal constituents for each record, and subtracting the model-derived currents. For example, for the zonal baroclinic current at the M_2 frequency

$$u = [a_o \cos(\omega t - \phi_o) - a_m \cos(\omega t - \phi_m)],$$

where o subscript refers to observed, and m refers to model parameters.

Assuming that these currents are typical for the entire

←

FIG. 6. Amplitude and phase derived from two 24-h CTD time series in May 1997 and Apr 1999. (a) Semidiurnal (solid lines) and diurnal (dashed lines) amplitudes from May 1997; (b) semidiurnal (solid circles) and diurnal (open stars) phases from May 1997; (c) as in (a), but for Apr 1999; (d) as in (b), but or Apr 1999.

TABLE 2. Barotropic kinetic and potential energies determined from model (J m^{-2}).

Tide	⟨KE⟩	⟨PE⟩
Semidiurnal	1578	747
Diurnal	420	3.9

TABLE 3. Baroclinic potential energies from CTD time series (J m^{-2}).

Tide	31 May 1997	16 Apr 1999
Semidiurnal ⟨PE⟩	782	75
Diurnal ⟨PE⟩	147	40
Barotropic ⟨KE⟩	1480	690

water column, one gets mean values over the array of 1337 and 829 J m^{-2} during 1996 and 1997, respectively (Table 4). Diurnal values are 403 and 323 J m^{-2}, respectively. Coefficients of variation for each year range from 11% to 97%, reflecting the variation seem in the tidal amplitudes.

Other researchers (Dushaw et al. 1995; Wunsch 1975) have assumed progressive wave characteristics for the baroclinic tide and used the ratio of potential to kinetic energy given by $(\omega^2 - f^2)/(\omega^2 + f^2)$. For these latitudes, this ratio is 0.33. Taking this value, and these estimates of kinetic energy, we obtain potential energy values around 400 J m^{-2}, which are about half the 1997 baroclinic potential energy estimates.

4. Summary and discussion

This study has made the first estimates of the stability of tidal currents over the Chatham Rise. In contrast to some earlier observations elsewhere (e.g., Magaard and McKee 1973), phase is stable in time and also is close to that of the modeled barotropic phase, while amplitudes show considerable variation. The Monte Carlo simulations show that the observed variability in tidal constituents cannot be explained simply by the presence of incoherent energy in the tidal band. Instead, phase variability is consistent with that expected given observed coherence levels, whereas amplitude variability is about twice that expected. This observation is consistent with the presence of a baroclinic tide phase locked to the barotropic tide, but having variable amplitude. Observations of vertical displacement up to 40 m tend to confirm the presence of baroclinic tide. Whether the baroclinic tide is being generated locally is impossible to determine from these results alone. The near-zero phase difference between the model and observations suggests the possibility of local generation.

Modulation of baroclinic tides has been observed near Hawaii by MC, and it is reasonable to suppose that the range in amplitude seen here is also a result of modulation. Mitchum and Chiswell attributed the modulation off Hawaii to changes in the deep thermal structure, which they suggest controls the efficiency of the barotropic to baroclinic tidal conversion. With the limited observations here, we can only point out that the thermal structure may play some role in the energy conversion because, although the barotropic semidiurnal energies in 1997 were double those of 1999, the baroclinic energies were 10 times higher.

The diurnal tide cannot exist as an internal wave at these latitudes (its turning latitude is ~30°S) so that, while energy could be put into diurnal tide locally, it is not likely to create a propagating wave. Presumably, however, the semidiurnal tide can propagate north of the rise, as seen off Hawaii, and it is interesting to note that both temperature sections along 178°30′E (Figs. 4a, 5a) shows oscillations that could be associated with baroclinic tides. The deep bowing of the isotherms centered at 41°S is associated with a semipermanent eddy, known as the Wairarapa Eddy (Roemmich and Sutton 1998), but the smaller fluctuations (e.g., those near 40°15′S and 42°15′S in 1997) could be due to baroclinic tide. These sections are too highly aliased in space and time to make accurate estimates of the period or wavelength.

This study is also the first that has made estimates of the baroclinic energetics over the Chatham Rise. With only two realizations of the semidiurnal tide in each CTD time series, and one realization of the diurnal tide, there cannot be much confidence in estimating long-term mean baroclinic tide levels from this study. In 1997, the average vertical displacement below the mixed layer was about 25 m (Fig. 6), whereas in 1999 it was 8 m. This approximately threefold difference in amplitude leads to the tenfold difference in potential energy levels between the two cruises.

The large range in computed energies makes it difficult to compare our results with those from elsewhere. The 1997 value of 782 J m^{-2} for the semidiurnal baroclinic potential energy is an order of magnitude or so higher than the 53 J m^{-2} Chiswell and Moore (1999) found for the flanks of the Kermadec Ridge, and the 104 J m^{-2} found by Feng et al. (1998) for the western Pacific Ocean. Thus these other studies tend to support our lower 1999 values as being more typical of energy levels near a ridge, yet they do not appear to have been in a region of active baroclinic tidal generation. Feng et al. (1998) reckoned that they were about 320 km from a generation site, and Chiswell and Moore's (1999) shallowest observations were in water 3000 m deep on the flanks of the Kermadec Ridge. The only other evidence we have that the 1997 levels may be typical is from the observations of Stanton (1977), who (although he did

TABLE 4. Baroclinic kinetic energies from current meter records (J m^{-2}).

	May 1996	Oct 1997
Semidiurnal ⟨KE⟩	1337 ± 68%	829 ± 97%
Diurnal ⟨KE⟩	402 ± 11%	323 ± 76%

not compute energy levels) reported vertical tidal displacements of 20 m near the shelf break off the west coast of New Zealand.

The baroclinic kinetic energies estimated here rely heavily on the assumption that the model produces an accurate barotropic tide and that the tidal analysis accurately estimates the coherent baroclinic tide. Given that the model produces amplitudes less than observed, but gets the phase right, it is possible that the model underestimates the barotropic tide amplitudes. If so, the energy estimates will be too low for the barotropic tide, and too high for the baroclinic tide. How well the baroclinic currents can be reconstructed using the tidal constituents is difficult to determine. Under the amplitude-varying phase-stable model invoked here, mean amplitudes (but not necessarily mean energies) will be reasonable well reconstructed. An alternative approach is to bandpass filter the records at each tidal period, and then subtract the model tide. Numbers so obtained depend on the width of the filter used, but typically are about twice those shown in Table 4. Presumably the bandpass filtering admits more incoherent energy than the approach taken here.

The results determined here raise the question: Can we estimate total radiation from the Chatham Rise? Energy radiation (flux) estimates depend on determining the speed at which the energy propagates. While it is unlikely that the baroclinic energy seen here is first baroclinic mode, the only estimate we have of this speed is the first baroclinic mode group velocity, c_g, which we calculate to be 0.4 m s^{-1}. If one makes the (probably unwarranted) assumption that the semidiurnal wave over the ridge is a progressive wave, the highest energy flux would be during 1997 when the total energy flux (PE + KE)*c_g is 1440 W m^{-1}. Taking the length of the Chatham Rise to be 750 km and assuming this value holds for the entire ridge, the total power radiated is about 1.1×10^9 W = 1.1 GW. The 1999 results suggest a value of 0.1 GW.

A radiated power of 1440 W m^{-1}, for all its uncertainty, is half of what Munk (1997, personal communication) suggests for a typical ridge and, even if this power is generated sporadically, the Chatham Rise could generate an appreciable amount of the world's total internal tide power. It seems that the tides here warrant more investigation.

Acknowledgments. I would like to thank all those who contributed to the cruises and made the collection of these data possible. Thanks are due to Phil Boyd, Kim Currie, Malcolm Greig, Peter Hill, Malcolm Hopkins, Bill Main, Sam McClatchie, Nils Oien, Dick Singleton, Phil Sutton, Matt Walkington, and Steve Wilcox for participation in data collection. Basil Stanton provided tidal ellipse calculation programs. Derek Goring provided the model output. Thanks are also due to the master and crew of R/V *Tangaroa* for their help at sea. I thank two anonymous reviewers for their comments. This work was carried out under Foundation of Research, Science and Technology Contracts CO 1422 and CO 1214.

REFERENCES

Baines, P. G., 1982: On internal tide generation in models. *Deep-Sea Res.,* **29,** 307–338.

Barnett, T. P., and R. L. Bernstein, 1975: Horizontal scales of mid-ocean internal tides. *J. Geophys. Res.,* **80,** 1962–1964.

Chiswell, S. M., 1994: Acoustic Doppler Current Profiler measurements over the Chatham Rise. *N. Z. J. Mar. Freshwater Res.,* **28,** 67–178.

——, and M. I. Moore, 1999: Internal tides in the southwest Pacific Ocean near Kermadec Ridge. *J. Phys. Oceanogr.,* **29,** 1019–1035.

——, M. Walkington, and B. R. Stanton, 1993: CTD data from Tasman-WOCE 1, NZOI cruise 3008, Akademik Lavrentyev, WOCE sections PR-13N, PR-11. NIWA Internal Rep.,85 pp. [Available from NIWA, P.O. Box 14-901, Wellington, New Zealand.]

Dushaw, B. D., P. F. Worcester, B. D. Cornuele, and B. M. Howe, 1995: Barotropic and baroclinic tides in the central North Pacific Ocean determined from long-range reciprocal acoustic transmissions. *J. Phys. Oceanogr.,* **25,** 631–647.

Feng, M., M. A. Merrifield, R. Pinkel, P. Hacker, A. J. Plueddemann, E. Firing, and R. Lukas, 1998: Semidiurnal tides observed in the western equatorial Pacific during the Tropical Ocean-Global Atmosphere Coupled Ocean–Atmosphere Response Experiment. *J. Geophys. Res.,* **103,** 10 263–10 272.

Heath, R. A., 1977: Phase distribution of tidal constituents around New Zealand. *N. Z. J. Mar. Freshwater Res.,* **11,** 383–392.

Hendry, R. M., 1977: Observations of the semidiurnal internal tide in the western North Atlantic Ocean. *Philos. Trans. Roy. Soc. London,* **286A,** 1–24.

Kantha, L. H., and C. Tierney, 1997: Global baroclinic tides. *Progress in Oceanography,* Vol. 40, Pergamon, 163–178.

Levine, M. D., and J. G. Richman, 1989: Extracting the internal tide from data: Methods and observations from the Mixed Layer Dynamics Experiment. *J. Geophys. Res.,* **94,** 8125–8134.

Magaard, L., and W. D. McKee, 1973: Semi-diurnal tidal currents at ''site D.'' *Deep-Sea Res.,* **20,** 997–1009.

Munk, W., and C. Wunsch, 1998: Abyssal recipes II. Energetics of the tides and wind. *Deep-Sea Res.,* **45,** 1976–2009.

Pugh, D. T., 1987: *Tides, Surges and Mean Sea-Level.* John Wiley and Sons, 472 pp.

Radok, R., W. Munk, and J. Isaacs, 1967: A note on mid-ocean internal tides. *Deep-Sea Res.,* **14,** 121–124.

Ray, R. D., and G. T. Mitchum, 1996: Surface manifestation of internal tides generated near Hawaii. *Geophys. Res. Lett.,* **23,** 2101–2104.

Roemmich, D., and P. J. H. Sutton, 1998: The mean and variability of ocean circulation past northern New Zealand: Determining the representativeness of hydrographic climatologies. *J. Geophys. Res.,* **103** (C6), 13 041–13 054.

Stanton, B. R., 1977: Preliminary observations of the internal tide over the shelf west of New Zealand. *N. Z. J. Mar. Freshwater Res.,* **11,** 703–712.

Walkington, C. M., and S. M. Chiswell, 1998: CTD data from NIWA cruise 3039: Ocean Fronts 1. NIWA Internal Rep., 107 pp. [Available from NIWA, P.O. Box 14-901, Wellington, New Zealand.]

Wunsch, C., 1975: Internal tides in the ocean. *Rev. Geophys. Space Phys.,* **13,** 167–182.